Materials & Design 232 (2023) 112101

Contents lists available at ScienceDirect

Materials & Design

journal homepage: www.elsevier.com/locate/matdes

4D direct laser writing of photo-triggered liquid crystal elastomer microactuators with large actuation strain

Zhenjia Huang [a], Gary Chi-Pong Tsui [a,*], Ka-Wai Yeung [a], Chun Li [a], Chak-Yin Tang [a], Mo Yang [b], Miao Zhang [c], Wai-Yeung Wong [c]

[a] Advanced Manufacturing Technology Research Centre, Department of Industrial and Systems Engineering, The Hong Kong Polytechnic University, Hung Hom, Kowloon, Hong Kong, China
[b] Department of Biomedical Engineering, The Hong Kong Polytechnic University, Hung Hom, Kowloon, Hong Kong, China
[c] Department of Applied Biology and Chemical Technology, The Hong Kong Polytechnic University, Hung Hom, Kowloon, Hong Kong, China

HIGHLIGHTS

- New conjugated polymers with high photothermal conversion efficiency (52.7%) and photostability were synthesized.
- Light-responsive conjugated polymers/liquid crystal photoresists with a room-temperature liquid crystal phase were developed for direct laser writing via two-photon polymerization.
- The incorporation of the 0.3 wt% conjugated polymers could lower the nematic-to-isotropic temperature of the LC photoresists to 48.0 °C.
- A large actuation strain (25.0%) of the 4D printed microactuator was achieved under the stimulation of near-infrared light with 808 nm wavelength.

GRAPHICAL ABSTRACT

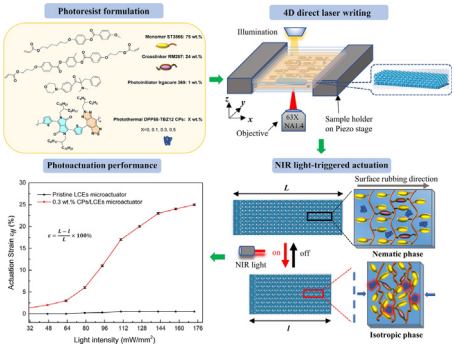

ARTICLE INFO

Article history:
Received 22 March 2023
Revised 31 May 2023
Accepted 14 June 2023
Available online 17 June 2023

Keywords:
4D direct laser writing
Microactuators
Conjugated polymers
Liquid crystal elastomers

ABSTRACT

4D printed photo-triggered liquid crystal elastomers (LCEs) microactuators by direct laser writing via two-photon polymerization (DLW-TPP) have attracted increasing attention due to their manipulation flexibility, reversible and rapid actuation capabilities. However, their development is hampered by the lack of room-temperature printable liquid crystal (LC) photoresists. Here, we developed new light-responsive LC photoresists by incorporating novel conjugated polymers (CPs) as photothermal agents for the DLW-TPP technology. The CPs displayed a remarkable photothermal effect and effectively avoided the aggregation problems that always happened for inorganic nanoparticles in photoresists. Moreover, the CPs incorporation lowered the nematic-to-isotropic temperature of the LC photoresists which is beneficial for room-temperature DLW-TPP. The printing parameters, including laser power and scanning speed, were investigated using the developed LC photoresists. It was found the range of printing parameters decreased with the increase of the CPs loading fraction from 0.1 to 0.5 wt%, which was attributed to

* Corresponding author.
E-mail address: mfgary@polyu.edu.hk (G.C.-P. Tsui).

https://doi.org/10.1016/j.matdes.2023.112101

the high photothermal conversion efficiency (52.7%). A well-defined CPs/LCEs microactuator with CPs as low as 0.3 wt% was printed, which could achieve a large 25.0% actuation strain in 5 s upon near-infrared (NIR) light stimulation. It could be used for thriving soft micro-robotics and micro-membranes with controllable separation capabilities.

1. Introduction

3D printing has shown remarkable advantages and promising applications thanks to its capacity to generate complex structures at different scales. When combined with stimuli-responsive materials, the printed structures can be equipped with dynamic property change over time in a controlled manner, which leads to the emerging 4D printing [1,2]. In the past decades, many studies have been performed to print time-dependent macroscopic structures with smart materials. However, the 4D printed structures at the microscale remain a challenge because of the difficulty of fabrication and the shortage of suitable smart materials. Among different printing techniques, direct laser writing via two-photon polymerization (DLW-TPP) is one of the powerful tools for producing precise and sophisticated structures at the micro and nanometer scale [3]. Relying on a nonlinear two-photon absorption (TPA) process, a femtosecond pulsed laser can be tightly confined into a small volume to initiate the selective polymerization of photosensitive mixtures (photoresists). Then true freeform structures with a high resolution can be generated [4]. It has been successfully used to fabricate microactuators that are applied in different fields, such as micro-robotics [5–7], micro-optics [8,9], and microfluidics [10].

Various stimuli-responsive materials, especially hydrogels [7,11,12] and liquid crystal elastomers (LCEs) [6,13–15], have greatly advanced the manufacturing of microactuators by DLW-TPP. Zheng et al. [16] fabricated microcantilevers using Poly(N-isopropylacrylamide) hydrogels with Fe_3O_4 nanoparticles. Two arms of the hydrogel actuator could close and open upon NIR light stimulation. Wang et al. [17] reported magnetic field-driven helical 3D microswimmers using gelatin methacryloyl/Fe_3O_4 nanoparticles, which exhibited a swimming behavior under rotation magnetic fields. Unfortunately, most hydrogel microactuators have low elastic modulus and are limited to requisite water environments. They need to expel water in and out for actuation, resulting in a slow response speed even on the order of minutes [18,19]. Liquid crystal elastomers, combining rubber elastomeric properties with liquid crystal (LC) orientational order, gain specific attention due to their reverse, large shape-morphing and quick response time on the order of seconds upon different stimuli, especially light (ultraviolet–visible (UV–vis) or near-infrared (NIR) light) [20]. Moreover, LCEs actuators do not necessarily need either external load or aqueous environments to conduct the shape deformations. For example, Dr. Keller first prepared temperature-responsive LCEs micro-pillars using the soft lithography method, which displayed large amplitude contractions [21,22]. These properties make LCEs an ideal choice for creating responsive microstructures with DLW-TPP technology. The deformation of LCEs microactuators is mainly controlled by the mesogenic alignment design, which can be programmed before polymerization. Upon external stimulus, the LCEs microactuator loses the nematic state, which leads to contraction along the long mesogen alignment direction and expansion in a perpendicular direction. Deformed LCEs return to their original shapes when the stimuli are removed due to the recovery of the mesogens. The most common-used alignment method for DLW-TPP is the boundary condition of micropatterned channels on the treated LC cell due to the thin thickness (typically <100 μm) of the microstructures [23].

The small scale of microactuators also makes light the most suitable stimulus due to the convenient manipulation, non-contact and spatiotemporal control via light wavelength and power. Light energy can be converted into mechanical work directly by isomerization change of azobenzene molecules [5,24] or indirectly through the photothermal effect of functional dopants [25]. Azobenzene-doped LCEs respond to UV for trans–cis isomerization and visible lights for cis–trans isomerization typically, which induces reversible deformation of the LCEs [26,27]. This reverse molecule configuration change was enormously applied in the macro-scale actuators until Zeng et al. [5] fabricated a UV-light-fueled microscopic walker by DLW-TPP. However, the periodical switching operation of dual-wavelength light for reversible deformation is not viable for many practical applications. Additionally, azobenzene-containing LCEs actuators have a low recovery speed from seconds to months [28,29].

In comparison, LCEs microactuators that use the photothermal effect display an obvious advantage. Photothermal dopants selectively absorb light, typically in the NIR region. And then, heat can be generated by the dopants to drive the nematic-to-isotropic phase transition of LCEs. Some problems exist in the development of LC photoresists with dopants for DLW-TPP. It is a critical issue to solve the dispersion quality and concentration of the dopants in photoresists. For instance, gold nanoparticles were treated with 3-mercaptopropionic acid [25], and multi-walled carbon nanotubes were acid-modified [30] for developing DLW-TPP-compatible LC photoresists. Inorganic nanomaterials must undergo surface chemical modification with functional groups before incorporation into LCEs. Nevertheless, poor compatibility makes most inorganic dopants prone to self-aggregate into larger ones and separate from the LC mixtures easily. Unwanted aggregation and separation generate uneven heating, which leads to unpredictable deformation behaviors of LCEs. A high concentration (1–10 wt%) of inorganic dopants is usually required for a favorable photothermal effect, which affects the printing process [31]. Therefore, high photothermal conversion efficiency, low doping ratio, and good dispersion of dopants in LC photoresists become crucial factors to be carefully considered in choosing the dopants for photothermal actuation of LCEs microactuators.

Conjugated polymers (CPs) have been widely applied in photothermal therapeutics recently [32]. Long electron donor–acceptor (D-A) backbones that contain contiguous sp^2- hybridized carbon atoms endow the CPs with a broad absorption in the NIR range, prominent photothermal effect, and high photothermal conversion efficiency [33]. They have obvious advantages over inorganic dopants and low-molecular organic dyes. Despite the superior photothermal property, the potential of CPs as dopants have been much less explored to create light-responsive LCEs microactuators. So far, only a handful of studies have reported film-like CPs-doped LCEs actuators. Liu et al. prepared polyaniline/LCEs films by heat polymerization, which could lift objects 200 times their weight under the NIR illumination [34]. This study pointed out the great potential of CPs as effective photothermal dopants in LCEs. Recently, Huang et al. incorporated CPs in LCEs to prepare ultrafast actuators by UV-photopolymerization with tunable deformation and motion under NIR laser irradiation [35]. However, there has been no report of the microactuators from

NIR light-responsive CPs/LC photoresists via 4D DLW-TPP technology.

Motivated by the above challenges, we aimed to develop a new light-responsive LC photoresist, which can be fabricated into NIR light-responsive 3D microactuators via room-temperature DLW-TPP technology. A novel planar DPP58-TBZ12 CPs with alternating D-A-type backbone structures was designed and synthesized as photothermal fillers. The DPP58-TBZ12 CPs exhibited a broad NIR absorption range and high photothermal conversion efficiency. They could be easily incorporated in the LC photoresists by organic solvent. Different LC photoresists with or without the CPs were carefully designed for the DLW-TPP technology. The effect of CPs content on the thermal property of the LC photoresist, printing parameter, and printing range during the DLW-TPP was investigated. It was found that a small amount of the CPs (0.3 wt%) in LCEs could not only lower the nematic-to-isotropic transition temperature value (T_{NI}) which was beneficial for 4D DLW-TPP microfabrication, but also yielded a fast response and large-scale actuation of the microactuators upon NIR light stimulation thanks to their superior photothermal effect. To the best of our knowledge, this is the first report of using CPs/LC photoresists with room temperature liquid crystal phases to manufacture microactuators by DLW-TPP technology without a heating stage.

2. Materials and methods

2.1. Materials and reagents

Tetrakis(triphenylphosphine)-palladium (0) ($Pd[PPh_3]_4$, 99%), phenylboronic acid pinacol ester (97%), and bromobenzene were acquired from Sigma-Aldrich. Toluene, chloroform-d, tetrahydrofuran (THF) (99.5%, extra dry) were bought from TiV Scientific Limited (Guangzhou, China). Toluene was dried over 4 Å molecular sieves. 4,8-Dibromo-6-(2-ethylhexyl)-[1,2,5]thiadiazolo[3,4f]benzotriazole (TBZ12) (98%) and 2,5-bis(2-octyldodecyl)-3,6-bis(5-(trimethylstannyl)thiophen-2-yl)-2,5-dihydropyrrolo[3,4-c]pyrrole-1,4-dione (DPP58) (98%) were bought from Derthon Optoelectronic Materials Science & Technology Co., Ltd. (Shenzhen, China). The liquid crystal monomer (LCM), 4-methoxybenzoic acid 4-(6-acryloyloxy-hexyloxy) phenyl ester (ST3866) and crosslinker 1,4-Bis-[4-(3-acryloyloxypropyloxy)benzoyloxy]-2-methylbenzene (RM257) and were purchased from SYNTHON Chemicals GmbH & Co. KG, Germany. The photoinitiator 2-Benzyl-2-dimethylamino-1-(4-morpholinophenyl)-1-butanone (Irgacure 369) was acquired from Sigma-Aldrich. The polyimide (PI) (Model DL-2590) was acquired from Shenzhen Dalton Electronic Material Co., Ltd., China. All the reagents and solvents were used directly without further purification unless otherwise noted.

2.2. NIR light-responsive photoresists design concept for DLW-TPP

An LC photoresist for DLW-TPP needs a stable LC phase at room temperature without an extra heating stage, which ensures the successful printing of simple or complex structures of a few hundred nanometers or micrometers that take different printing times. To date, reactive LC photoresists with room-temperature liquid crystal phases are rare. The LC phases of most reported LC mixtures exist above room temperature, and LC mixtures crystallize easily in the ambient environment in a short time. Thus, it is challenging to prepare DLW-TPP-compatible LC photoresists. Particularly, LC mixtures with light (UV–vis and NIR)-responsive dopants have seldom been developed. According to our previous studies [25,35,36], ST3866 with monoacrylate mesogens was selected as the LC monomer to provide flexibility for the network. To fabricate stable LCEs structures, RM257 (T_{NI} = 129 °C) containing diacrylate mesogens was chosen as the crosslinker to form the network and fix the alignment. Irgacure 369 was chosen as the photoinitiators. It has been used in other studies to generate radicals in acrylate-based photoresists. It is known that LC photoresists of higher T_{NI} may suffer some degrees of crystallization, which is unbeneficial to the DLW-TPP microfabrication [36–38]. The weight percentage between the monomer and crosslinker was investigated to determine the T_{NI} of different LC photoresists.

The photothermal dopants should not destroy the mesogenic alignment and should be transparent or semitransparent to the femtosecond laser [31]. A planar alternating donor–acceptor (D-A) conjugated polymers exhibit many advantages as photothermal materials, including ease of synthesis, unique temperature tunability from NIR light, lightweight, and good biocompatibility. It has been demonstrated that D-A_1-D-A_2-type CPs possess a lower band gap energy, resulting in absorption in the NIR region. Diketopyrrolopyrrole (DPP) represents an electron-acceptor due to its electron-deficient nature, which makes it suitable for use as a bridging moiety in D-A-type CPs. Its copolymerization with aromatic heterocycles, such as bithiophene, has been applied in the Stille cross-coupling polymerization [33]. The introduction of branched or linear alkyl side chains into CPs can help improve the solubility in organic solvents, while not influencing the alternating backbone [39]. Therefore, in this work, DPP58 containing thiophene as donor and DPP as acceptor 1, and TBZ12 containing thiadiazolobenzotriazole as acceptor 2, are chosen as the two monomers for the synthesis of the CPs, named DPP58-TBZ12. The conjugated polymer DPP58-TBZ12 was then incorporated into the LC photoresists as an effective photothermal agent responsive to NIR light irradiation. DPP58-TBZ12 CPs and LC photoresists show good solubility in THF, which makes it easy to obtain homogenous mixtures after evaporating the THF solvent. Because the thickness of the microstructures by DLW-TPP is less than 100 μm, the method for mesogenic alignments was achieved by the micropattern-boundary conditions of unidirectional rubbing PI-coated glass.

2.3. Synthesis and characterization of DPP58-TBZ12 CPs

The DPP58-TBZ12 conjugated polymers were synthesized following our previous work [35]. The synthesis routine through Stille cross-coupling polymerization is shown in Scheme 1. Briefly, a solution of electronic donor DPP58 (monomer 1, 119 mg, 0.1 mmol), and electronic acceptor TBZ12 (monomer 2, 44.7 mg, 0.1 mmol) and palladium catalyst $Pd[PPh_3]_4$ (10 mg, 0.008 mmol) were placed in a 25 mL of Schlenk tube. Next, 10 mL of anhydrous toluene was added. All these procedures were completed in a glove box to avoid oxygen. The solution was stirred vigorously at 100 °C. After 48 h reaction time, 1 mL of phenylboronic acid pinacol ester (8 mg, dissolved in toluene) and 0.1 mL of bromobenzene were dropped into mixtures to eliminate the end groups separately under the protection of the nitrogen atmosphere. The reaction continued for 20 min. After the solution was cooled to room temperature, methanol (100 mL) was used to precipitate the resulting substance. The precipitates were then collected using filter paper. To purify the crude powder, it was subjected to Soxhlet extraction with methanol and acetone for 24 h. The extraction could clear away low molecular weight polymers and $Pd[PPh_3]_4$ in the products. The resultant product was collected and dried at 45 °C under a vacuum for 24 h to yield blue DPP58-TBZ12 CPs (205 mg, 70% yield). ^{1}H NMR (400 MHz, $CDCl_3$, δ): 9.33–9.11 (br, 4H),7.59–7.38 (br, 4H), 5.01 (br, 2H), 4.27–4.12 (br, 2H), 2.30 (br, 1H), 1.58–0.84 (br, 90H). Molecular weight was measured by GPC as M_n = 10240 g/mol; M_w = 11759 g/mol; polydispersity index (PDI) = 1.15.

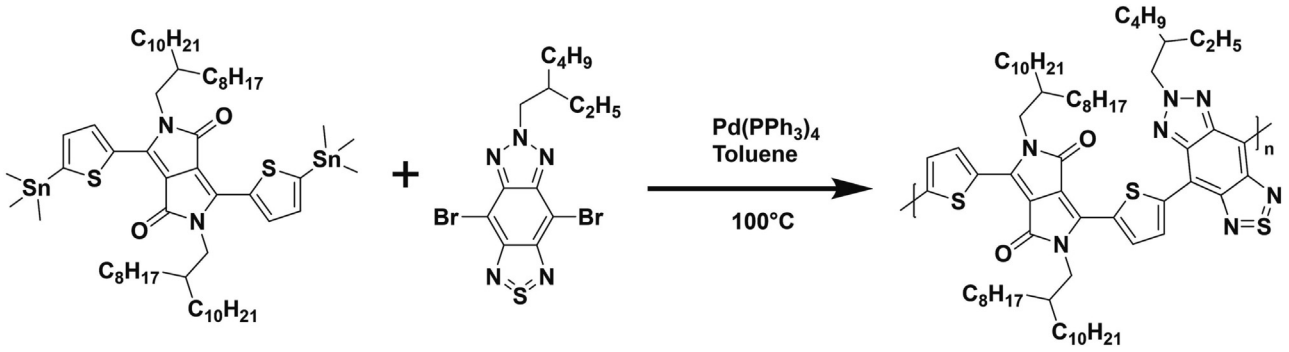

Scheme 1. Schematic of the synthetic route of conjugated polymers DPP58-TBZ12.

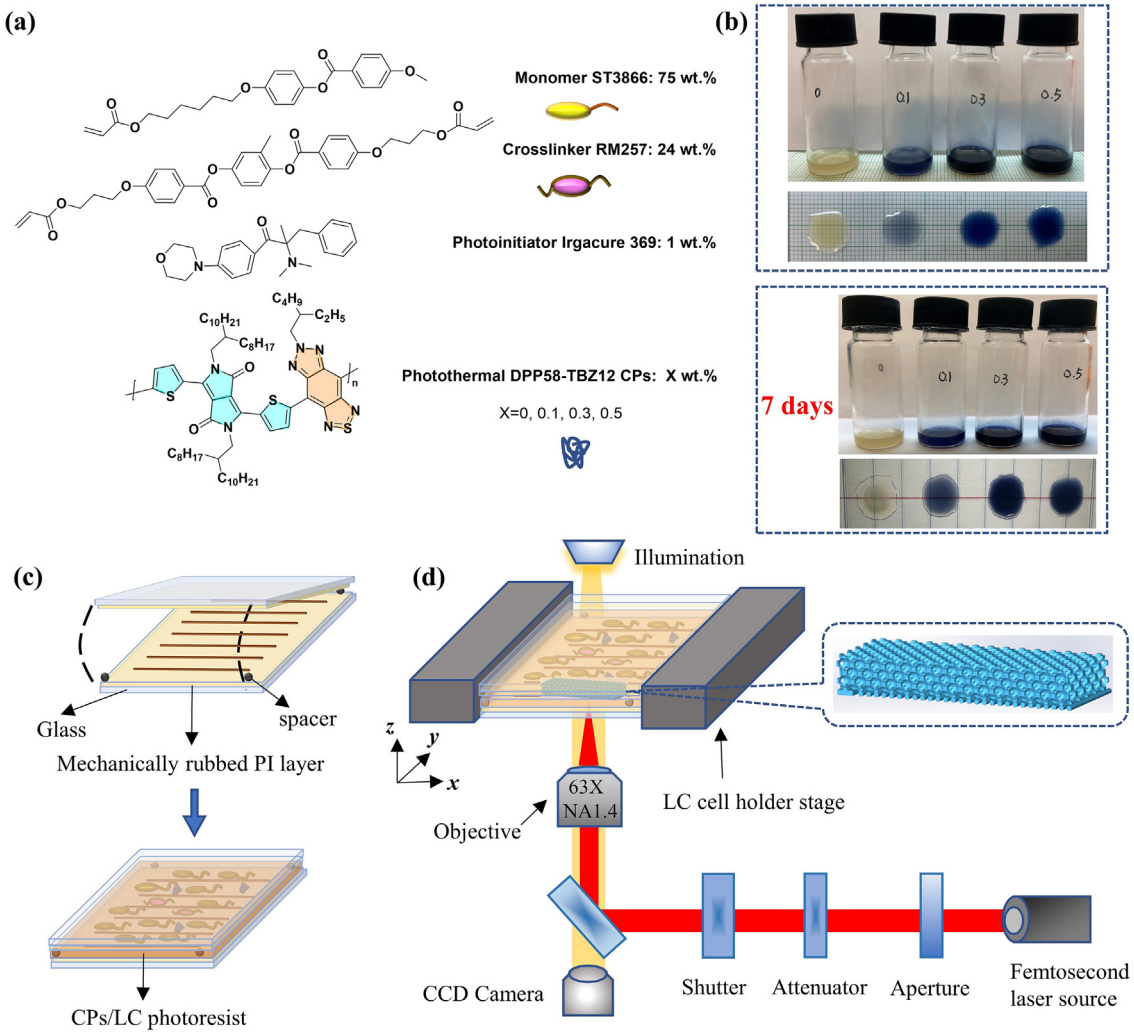

Fig. 1. (a) Chemical structures of LC monomer ST3866, crosslinker RM257, photoinitiator Irgacure 369, and dopant DPP58-TBZ12 CPs. (b) Images of the prepared LC photoresists with 0, 0.1 wt%, 0.3 wt%, and 0.5 wt% DPP58-TBZ12 CPs on the first and seventh days. (c) Schematic illustration of liquid crystal cell assembly and a typical liquid crystal cell filled by DPP58-TBZ12 CPs/LC photoresists. (d) The schematic diagram of oil immersion configuration in DLW-TPP setup for fabricating microstructures.

2.4. Preparation of the DPP58-TBZ12 CPs/LC photoresists

The CPs/LC photoresists were prepared according to the following process. The chemical structures are shown in Fig. 1a. Different amounts of as-synthesized conjugated polymers DPP58-TBZ12 were ultrasonically dissolved into THF solvent in a vial. Then 75 wt% ST3866 as the LC monomers, 24 wt% RM257 as crosslinkers and 1 wt% Irgacure 369 as the free radical photoinitiators were added to the solution. The mixtures stored in an open vial were stirred gently at 65 °C for 12 h to eliminate the THF solvent thoroughly. These LC photoresists were produced with different contents of DPP58-TBZ12 CPs: 0, 0.1, 0.3, 0.5 wt% for subsequent photopolymerization of 3D microstructures. Fig. 1b exhibits that the DPP58-TBZ12 CPs are well-dispersed in the LC photoresists.

After storage in a dark place for 7 days, crystallization occurred somewhat in the pristine LC photoresist. The CPs-doped photoresist maintained good stability and high dispersion without evident CPs aggregates and crystallization behavior, making these photoresists suitable for printing. It is significant to note that the high dispersion capability and good compatibility of DPP58-TBZ12 CPs within LCEs can ensure the successful printing of NIR light-responsive microactuators by DLW-TPP.

2.5. Liquid crystal cells construction

The sandwich-like liquid crystal cell was assembled based on commonly utilized approaches to achieve the uniaxial alignment of the mesogens [25]. To elaborate, two glasses used for LC cells were washed by successive immersion in acetone and methanol. PI was spin-coated on the glass substrate for planar surface alignment (parallel to the substrate) at 1500 rpm for 40 s, followed by curing on a 120 °C stage for 3 min. A velvet cloth was employed to mechanically rub the PI-coated glasses to obtain a micro-grooved surface for the mesogen alignment. Finally, a homemade LC cell was constructed by carefully assembling two rubbed PI-coated substrates with antiparallel alignment direction on two inner sides gapped via spherical spacers (55 μm diameter) in UV-curable glue. The prepared photoresists were heated to reach the isotropic phase at 60 °C above their T_{NI}. Subsequently, they were injected into the homemade aligned LC cells from the edge through capillary force to avoid flow-induced alignment (Fig. 1c). The LC cells were then cooled to room temperature at a controlled rate (5 °C/min). Finally, an LC cell filled by ordered nematic phase photoresists was constructed well for DLW-TPP. Notably, a low cooling rate is vital to reduce the number of disclinations [9]. The alignment of mesogens was checked with a polarized optical microscope. Finally, user-designed 3D microstructures or other samples were produced by DLW-TPP or UV light exposure (1.2 mW/cm^2, 365 nm).

2.6. DLW-TPP setup

A commercially available DLW-TPP equipment (Nanoscribe Photonic Professional, GmbH, Germany) was employed to fabricate 3D microstructures. A Ti: sapphire femtosecond laser with a central wavelength of 780 nm (pulse duration of approximately 100 fs, a repetition rate of 80 MHz, and a maximum power of 180 mW) was utilized in this equipment. The laser beam was focused into the CPs/LC photoresists using a 63x oil-immersion objective lens (Zeiss, NA = 1.4). The schematic diagram of the DLW-TPP setup is shown in Fig. 1d. When the power was adjusted to a scaling factor of 1, the average laser output within the focal region was 50 mW. All 3D microstructures were designed by computer-aided design software (Solidworks). The sample cell was fixed on the *XYZ* positioning stage controlled by combined modes (galvo mode for *x- and y-axes* and piezo mode for the *z-axis*). After bottom-up DLW-TPP microfabrication, the cell was separated, and the glass substrate with microstructures was dipped in acetone for 6 min to remove the unpolymerized photoresist. The desired self-standing 3D microactuators on the glass substrates were achieved by drying with gentle nitrogen flow.

2.7. NIR photothermal properties of DPP58-TBZ12 CPs

The photothermal properties of synthesized DPP58-TBZ12 CPs were measured by a NIR laser setup (LSR808H-2 W, Lasever Inc., Ningbo, China) with a wavelength of 808 nm and a laser power of 0.5 W. The beam spot size at the aperture is 4.8 × 5.3 mm^2. The distance between the NIR light source and the CPs dispersion was maintained at 20 cm. The temperature change of samples was recorded using a FLIR C3-X thermal camera (FLIR Systems OU, Estonia). To determine the photothermal conversion efficiency (PCE) of DPP58-TBZ12 CPs, 0.05 mg/mL samples in o-xylene were irradiated by the NIR laser at 0.5 W for 5 min to reach a saturation temperature and then cooled down to room temperature with the laser switched off. The temperature of the CPs dispersion was monitored at an interval of 5 s during this cooling period. A total of five heating and cooling cycles was carried out to evaluate the photothermal stability of the DPP58-TBZ12 CPs.

Photothermal conversion efficiency (η, %) of DPP58-TBZ12 CPs was calculated by the following equations deriving from Roper's report [40];

$$\eta = \frac{hS(T_{max} - T_{amb}) - Q_{dis}}{I(1 - 10^{-A_{808}})} \tag{1}$$

where h is the heat transfer coefficient, S is the surface area of the container, T_{max} and T_{amb} are saturation temperature (also the maximum system temperature) of the irradiated sample and the environment temperature. Q_{dis} represents heat dissipated from light absorbed by the sample container and o-xylene solvent, and it is measured independently using a container containing o-xylene without CPs. I means the incident laser power. A_{808} is the absorbance (0.873) of the CPs dispersion at 808 nm. The value of hS can be calculated from the equation:

$$hS = \frac{mC_{OX}}{\tau_s} \tag{2}$$

where m is the mass of the solution containing the CPs (0.2 g), $C_{o-xylene}$ express the specific heat capacity of the o-xylene solvent ($C_{o-xylene}$ = 1.26 J/(g×°C)), and τ_s represents the slope of the linear time data vs negative natural logarithm of driving force temperature.

$$t = -\tau_s \ln(\theta) \tag{3}$$

where θ is introduced to define a parameter.

$$\theta = \frac{T_t - T_{amb}}{T_{max} - T_{amb}} \tag{4}$$

T_{max} and T_{amb} represent the steady-state temperature of the CPs and the environment temperature. T_t is the corresponding temperature of DPP58-TBZ12 CPs during the cooling process.

2.8. Characterizations

To determine the chemical structures of the synthesized DPP58-TBZ12 CPs, ^{1}H nuclear magnetic resonance (^{1}H NMR) spectroscopy was carried out on a Bruker Avance-III 400 MHz spectrometer. Chemical shifts were recorded in parts per million (ppm) and were referenced as residual chloroform-d ($CDCl_3$) (δ_H = 7.26 ppm) as the internal standard. Attenuated total reflectance Fourier-transform infrared spectroscopy (ATR-FTIR) measurement was conducted using a Thermo Scientific Nicolet IS50 Spectrometer with an advanced XT-KBr Gold spectrometer at a room temperature in the range of 400–4000 cm^{-1}. Gel permeation chromatography (GPC) (Agilent GPC 50) was used to evaluate the number average molecular weight (Mn), weight average molecular weight (Mw), and polydispersity index (PDI) of the DPP58-TBZ12 CPs·THF was the eluent, and narrowly distributed polystyrene was used as the standard. A Shimadzu UV–vis spectrophotometer (Kyoto, Japan) was used to investigate the UV–Vis-NIR absorption spectra of the synthesized CPs.

The nematic-to-isotropic transition temperature (T_{NI}) of the LC photoresists was determined by differential scanning calorimetry (DSC) (Mettler Tolede, DSC3). LC or CPs/LC photoresists of at least 3 mg were aced into aluminum pans. Subsequently, samples were

heated and cooled from 20 °C to 120 °C at a ramping rate of 10 °C/min under nitrogen protection. Two cycles were performed, and the results in the second cycle were recorded. Thermogravimetric analysis (TGA) was conducted on a Mettler Toledo TGA/DSC 3+ at a heating rate of 10 °C/min from 25 to 650 °C. UV-polymerized pristine LCEs and CPs/LCEs films were chosen as the TGA samples. Investigation of the main printing parameter window for newly developed photoresists was critical for the morphology and integrity of 4D printing structures and manufacturing time. Laser powers varying from 3.5 to 21 mW and scanning speeds ranging from 2 to 24 mm/s were assessed in the DLW-TPP process. A field-emission scanning electron microscope (SEM) (Tescan VEGA3, Czech Republic) was applied to observe and analyze the fabricated 3D DPP58-TBZ12 CPs/LCEs microstructures at an acceleration voltage of 20 kV after sputter-coating them with 10 nm gold layer. A polarized optical microscope (POM) (Zeiss Axiolab 5) equipped with a hot stage was employed to examine the bright field images of LC photoresists and cross-polarized microscope images of LCEs microstructures.

NIR light-induced actuation of DPP58-TBZ12 CPs/LCEs microactuators was performed using the NIR laser setup of 808 nm (LSR808H-2 W, Lasever Inc., Ningbo, China). The beam spot size of the NIR laser is 4.8 × 5.3 mm^2. The output laser powers could be adjusted from 0.1 W to 5 W. The corresponding power intensity can be adjusted from 4 to 197 mW/mm^2. The deformed microactuators and videos were recorded by a CCD camera with an optical microscope.

3. Results and discussions

3.1. Characterizations of DPP58-TBZ12 CPs

The chemical structure of the prepared DPP58-TBZ12 CPs was confirmed by ^{1}H NMR spectra and ATR-FTIR. ^{1}H NMR spectra are shown in Fig. 2a. All characteristic peaks are corresponding to their related hydrogen atoms according to chemical shift, integral area, and coupling constant. The multiple peaks at 0.84–1.58 ppm were ascribed to the aliphatic protons of the alkyl side chains of DPP58 and TBZ12 units. Characteristic peaks from 7.38 and 7.59 ppm were corresponding to the aromatic protons in TBZ12. The peaks at 9.11 and 9.33 ppm were related to the protons of the thiophene moieties in DPP58. The observed chemical shift was consistent with the proton position in the conjugated polymer DPP58-TBZ12 structure. The ^{1}H NMR results indicate the D-A DPP58-TBZ12 conjugated polymers were synthesized with success through Stille cross-coupling polymerization.

The ATR-FTIR spectra for the CPs were conducted in the range of 4000–400 cm^{-1}, as depicted in Fig. 2b. Several characteristic peaks of each are identified. The absorption peak at 2935 cm^{-1} and 2862 cm^{-1} were ascribed to the asymmetrical stretching vibrations of the aliphatic C-H and the symmetrical stretching vibration of the saturated C-H bonds, respectively [41]. The peaks confirmed the construction of a conjugated skeleton during the polymerization. The strong absorption peaks around 1664 cm^{-1} and 1550 cm^{-1} were related to the C═O and C═C in stretching vibration in DPP58 and TBZ12 rings, respectively. The peak at 1143 cm^{-1} belongs to the stretching vibration of N-N bonds on the TBZ12 ring. The peak at 1109 cm^{-1}, 1079 $cm^{-1,}$ and 1023 cm^{-1} were assigned to the C-N and N-N stretching vibration in the TBZ12 ring. 846 cm^{-1} was associated with the out-of-plane vibration of the C-H bonds of the acrylate group. Due to the small incorporation of CPs in the LCEs matrix and similar feature functional groups, no new feature peaks were observed in the CPs/LCEs film spectra compared to the CPs spectra.

The planar DPP58 monomers contain two electron-rich thiophene rings and an electron-deficient core diketopyrrolopyrrole. The TBZ12 monomers serve as an electron-deficient acceptor. Due to the alternating planar D-A_1-D-A_2 backbone, DPP58-TBZ12 CPs exhibited a low band gap, resulting in a broad absorption range between 600 nm and 800 nm in THF solution with a peak located around 746 nm (Fig. 2c). The absorption behavior of the CPs around the NIR region was beneficial for the preparation of NIR light-responsive photoresists.

3.2. NIR photothermal properties of DPP58-TBZ12 CPs

As exhibited in Fig. 3a and b, no distinct temperature change was observed for o-xylene after 5 min NIR light stimulation. On the contrary, the temperature of the 0.05 mg/mL DPP58-TBZ12 CPs dispersion showed an obvious and quick rise from 18 to 79.2 °C, which confirmed the effective photothermal conversion ability. According to the experimental results and equations (1) - (4), the time constant for heat transfer from the sample solution was calculated to beτ_s = 69.63 by using the linear time data from the cooling period vs. the negative natural logarithm of driving force temperature (Fig. 3c). *hA* was calculated to be 3.6 × 10^{-3} W/°C. Then a high photothermal conversion efficiency (η) value of DPP58-TBZ12 CPs could be acquired to be 52.7%, compared with other reported photothermal CPs [42–44]. To evaluate the photothermal stability of the CPs, which is a critical evaluation parameter in NIR photoactuation, the recyclable temperature change in the presence of the CPs under NIR light on and off is shown in Fig. 3d. The CPs dispersion was irradiated under 808 nm light of 0.5 W for 300 s and cooled down to the room temperature by turning off NIR light. During at least five heating and natural cooling cycles, the maximum temperature of DPP58-TBZ12 CPs was almost constant, demonstrating their admirable photothermal conversion stability.

3.3. Thermal properties of DPP58-TBZ12 CPs/LC photoresists

Before the addition of NIR-absorbing species, the T_{NI} values of LC photoresists with the different weight ratios of ST3866: RM257 were investigated. DSC results show that the T_{NI} values of the LC photoresists decrease with the increasing weight ratio of the diacrylate crosslinker RM257, as listed in Table 1. They exhibited a wide temperature range to keep the nematic phase. In comparison, the LC photoresist 3 with a low crosslinker concentration was chosen because of the low T_{NI} for room-temperature 4D printing and the relatively low stiffness of the polymeric network for actuation upon stimulation. Fig. 4a presents the results of DSC measurement in the second heating process after erasing the thermal memory of the pre-polymerized LC and DPP58-TBZ12 CPs/LC photoresists. The heat flux with temperature for these pre-polymerized mixtures displayed only the nematic-isotropic transition (T_{NI}). The T_{NI} of unfilled LC and CPs/LC photoresists with 0.1, 0.3, 0.5 wt% of DPP58-TBZ12 CPs are 55.1, 51.4, 48.0, and 45.2 °C, respectively. T_{NI} of blank nematic LC photoresists is about 55.1 °C, while those of the DPP58-TBZ12 CPs/LC photoresists are lower. The DSC results indicated that the T_{NI} value of CPs/LC photoresists dropped largely with the content increase of DPP58-TBZ12 CPs. Because photopolymerization and crosslinking of LC photoresists are required to occur in the nematic state for later NIR photothermal actuation, the temperature for performing DLW-TPP should be in the range of the nematic phase temperature. The room temperature below the T_{NI} satisfies the printing temperature requirement of DLW-TPP for these photoresists.

The crossed polarized micrographs of 0.3 wt% CPs/LC photoresists at 25 and 60 °C depicted the nematic and isotropic phases,

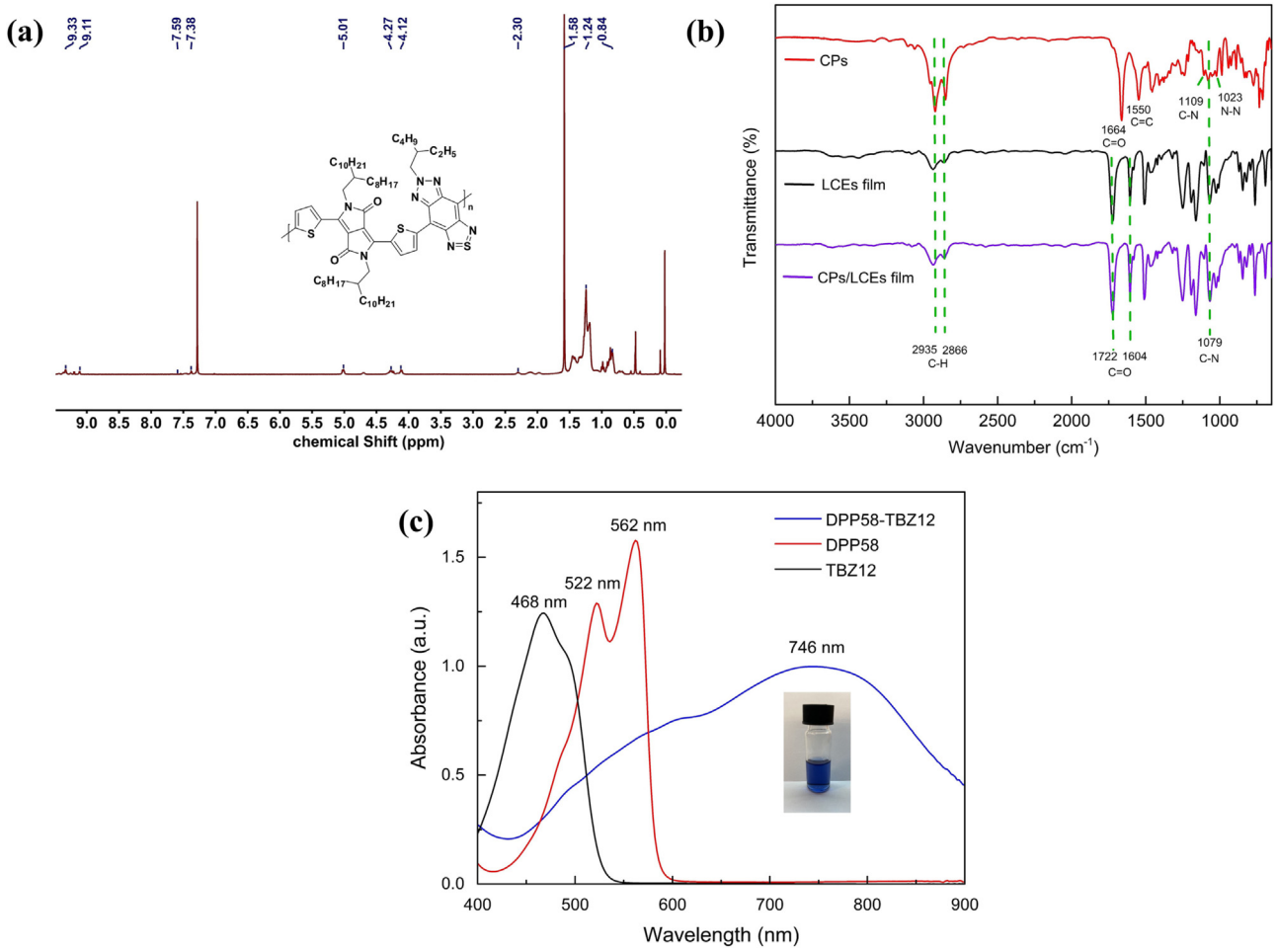

Fig. 2. (a) ^{1}H NMR spectra (400 MHz) of the DPP58-TBZ12 CPs in $CDCl_3$. (b) ATR-FTIR spectroscopy of the DPP58-TBZ12 CPs, LCEs film, and CPs/LCEs film. (c) UV–Vis-NIR absorption spectra of DPP58, TBZ12, and DPP58-TBZ12 CPs (concentration = 0.05 mg/mL, dissolved in THF) (Insert: the photography of 0.05 mg/mL DPP58-TBZ12 CPs in THF solution).

respectively. A clear schlieren texture was visible when the LC mixtures were cooled to room temperature that was below the transition temperature T_{NI} (48.0 °C) (Fig. 4b). The mechanism might be attributed to two reasons: (a) diminished strength of intermolecular forces between rigid rod-shaped mesogens due to the insertion of planar CPs; (b) the thermal–mechanical response of the planar CPs [45–47]. These effects of the DPP58-TBZ12 CPs might lead to a more manageable disturbance of nematic arrangement between mesogens and lower T_{NI} values. It is worth noting that the LC photoresists containing the CPs with lower T_{NI} have longer and more stable periods in a defect-free nematic phase at room temperature. The influence of DPP58-TBZ12 CPs on the T_{NI} of LC mixtures also may alleviate some degree of crystallization during the DLW-TPP fabrication. TGA was performed to investigate the mass loss of the UV-photopolymerized samples of pristine LCEs and CPs/LCEs films. The TGA curves exhibit that the pristine and the DPP58-TBZ12 CPs incorporated LCEs films had high thermal stabilities. The decomposition of these films did not occur until the temperature reached approximately 340 °C (Fig. 4c).

3.4. Printing parameters of DLW-TPP for DPP58-TBZ12 CPs/LC photoresists

The printing capacity of DLW-TPP in the micro and nanoscale enables the complexity and diversity of the designed structures. The developed CPs/LC photoresists allow a wide range of printing parameters, including laser power and scan speed. It is significant to tune these two main printing parameters to ensure the final quality and manufacturing efficiency of the printing structures. Laser power determines the throughput of photons in the focal volume within the photoresist, while the scanning speed regulates the photon dose [25]. A suitable laser power should meet the requirements that it can initiate the polymerization and does not exceed the burning threshold to generate structures matched with the designed 3D model. A low laser power leads to incomplete polymerization and crosslink of the LCEs, further leading to collapsed structures. In addition, the photothermal effect of the CPs in the printing process also needs to be considered in determining the suitable laser power. The filled DPP58-TBZ12 CPs could absorb the femtosecond laser energy and likely result in localized burning and bubbling of the photoresist in a very short time during the manufacturing process, particularly evident with slow scan speed. Although the laser power is very low, unwanted heat energy could still make the printing layers swell and influence the fidelity of the designed model.

In this case, a porous inverse opal structure unit with pore size of 3.7 μm radius was designed as the model for the parameter selection of as-prepared DPP58-TBZ12 CPs/LC photoresists (Fig. 5a). In the DLW-TPP manufacturing process, a hatching distance of 0.2 μm and a slicing distance of 0.3 μm was adopted. The laser power varied between 3.5, 7, 10.5, 14, 17.5, and 21 mW, and the scanning speed was adjusted between 2, 4, 6, 8, 10,

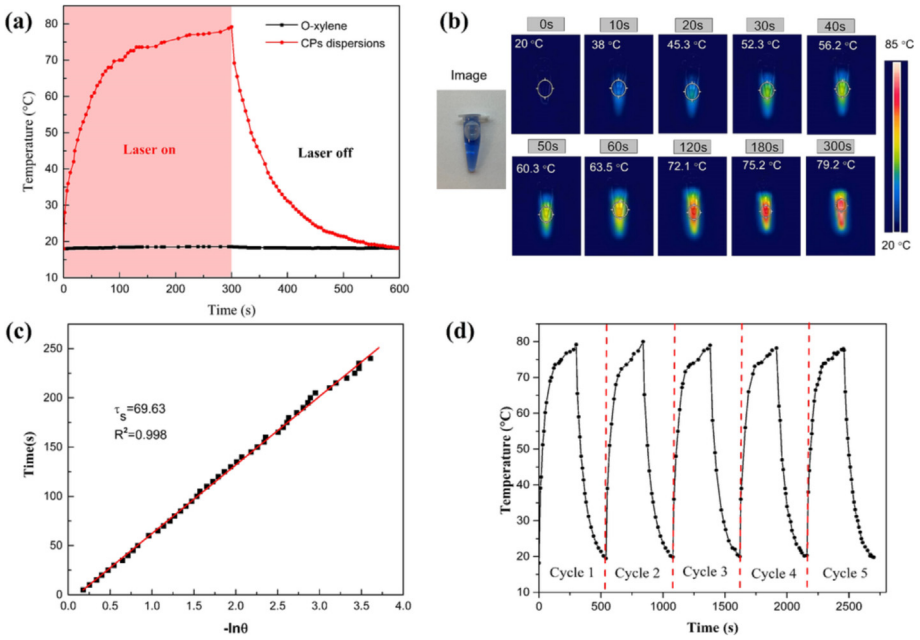

Fig. 3. (a) Time-dependent temperature change curves of 0.05 mg/mL DPP58-TBZ12 CPs in o-xylene under a NIR laser irradiation (808 nm, 0.5 W), and the laser was turned off after 5 min. (b) Infrared thermal images of 0.05 mg/mL DPP58-TBZ12 CPs solution with laser irradiation at different times. (c) The linear plot of cooling time versus the negative natural logarithm of driving force temperature for determining photothermal conversion efficiency. (d) Stability study of the DPP58-TBZ12 CPs dispersions under five photothermal heating and natural cooling cycles.

Table 1
Phase transition temperature for LC photoresists (wt.% of the total mixture).

Photoresists	Monomer ST3866	Crosslinker RM257	Photoinitiator Irgacure 369	T_{NI} (°C)
LC Photoresist 1	35	64	1	77.7
LC Photoresist 2	55	44	1	65.6
LC Photoresist 3	75	24	1	55.1

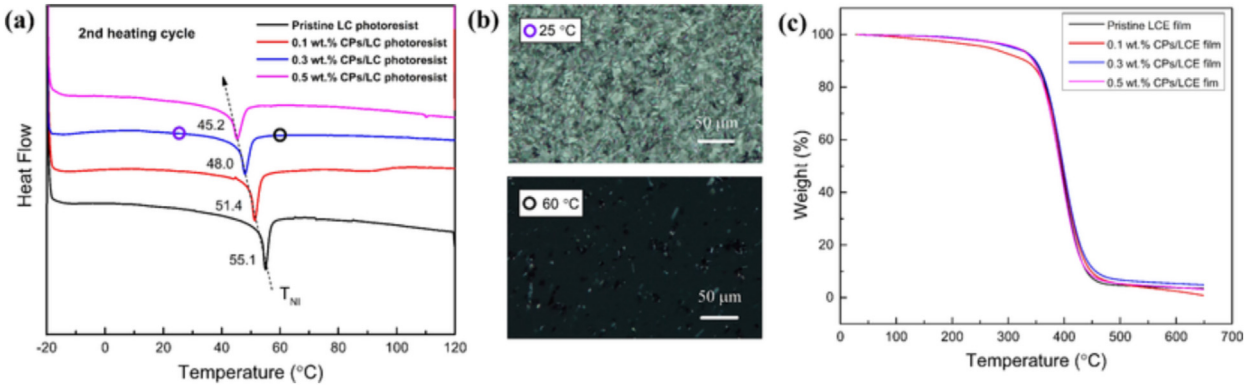

Fig. 4. (a) DSC thermograms of pristine LC photoresists and DPP58-TBZ12 CPs/LC photoresists in the second heating cycle at a rate of 10 °C/min under the protection of nitrogen. (b) Crossed polarized micrographs of the 0.3 wt% CPs/LC photoresist taken below (25 °C, top) and above (60 °C, bottom) the T_{NI} between uncoated glasses. (c) TGA results of the pristine LCEs and CPs/LCEs films with different doping ratios of the CPs.

14, 16, 20, and 24 mm/s. LC photoresists incorporated with 0.3 wt% and 0.5 wt% CPs were employed to explore the influence of photothermal filler amounts. Two matrixes with 54 micro inverse opal units were printed with different parameters. Suitable printing windows with appropriate laser power and scanning speed define acceptable structures with well-recognizable clarity visually. The side effect of heat energy was aggravated by increasing the concentration of DPP58-TBZ12 CPs in photoresists during the DLW-TPP process, which made the printing window narrow for printing parameters selection (Fig. 5b and c). Although the CPs absorb 746 nm laser light, expansion during the printing process can be avoided by choosing suitable printing parameters in the wide printing window. From these results of printing parameters and CPs concentration, a laser power of 7 mW and a scanning speed of 10 mm/s were adopted as suitable experimental printing parameters for generating CPs/LCEs microstructures. LC photoresists with 0.3 wt% CPs were chosen as the material for 4D DLW-TPP technology.

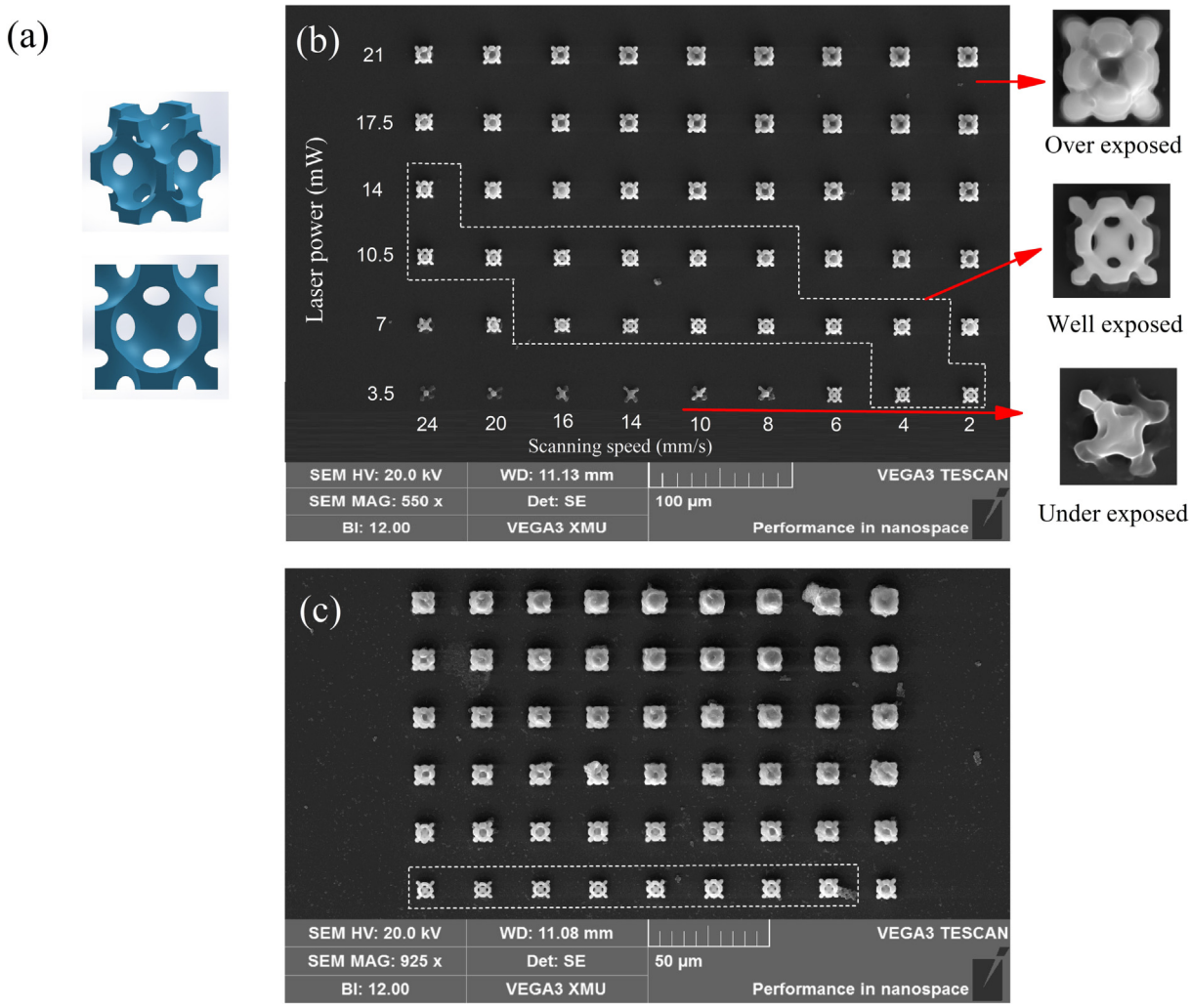

Fig. 5. (a) 3D model design of an inverse opal structure unit with 3.7 µm radius. (b) Scanning electron microscopic (SEM) images of 0.3 wt% CPs/LCEs microstructures fabricated using DLW-TPP technology at varying laser powers (from 3.5 to 21 mW at an interval of 3.5 mW) and varying scanning speeds (2, 4, 6, 8, 10, 14, 16, 20, 24 mm/s). Under-exposed, well-exposed, and over-exposed microstructures were also displayed to determine printing windows. (c) SEM images of 0.5 wt% CPs/LCEs microstructures fabricated using DLW-TPP with the same varying laser powers and scanning speeds.

3.5. NIR photothermal actuation of the microactuators

To demonstrate the NIR light-induced actuation capabilities of a microactuator fabricated with the developed photoresists, a porous NIR light-driven LCEs microactuator (150 µm × 50 µm × 20 µm) composed of two layers of 3D inverse opal structure with 3.7 µm radius was fabricated by DLW-TPP using the 0.3 wt% CPs/LC photoresist (Fig. 6a). The SEM image of the printed structure is shown in Fig. 6b, which is consistent with the designed model. The alignment of the rigid mesogens on the PI-coated substrate was verified through the polarized optical microscope (POM) with the printed microstructures placed between crossed polarizers. There is a clear difference in the molecular orientation-induced birefringence of the CPs/LCEs microstructures under polarized light. The porous scaffold appeared dark when the rubbing direction aligned parallel to either the polarizer or analyzer (Fig. 6c). In contrast, the scaffold turned bright when the rubbing direction was rotated at 45° to the polarizer (Fig. 6d). The difference demonstrates that the printed microstructures comprise the homogeneous orientation of the mesogens along the rubbing direction.

The microactuator showed a large anisotropic shape change upon NIR light irradiation, which contracted and expanded along parallel ($l_{\parallel}$) and perpendicular ($l_{\perp}$) to the alignment direction, respectively. The anisotropic photothermal response in different directions is characteristic of uniaxially aligned polymerized networks. Interface adhesion between the microactuator and the glass substrate has a great influence on axial deformation. Therefore, specific cylindric supporters with 3 µm of diameter are designed to reduce the adhesion of the microactuator for light-induced actuation after development. The photo-triggered actuation was investigated by placing the developed microactuators on the glass substrate. Upon NIR light irradiation with the wavelength of 808 nm, the local temperature will increase quickly to disorder the mesogen arrangement of the LCEs due to the photothermal conversion ability of the DPP58-TBZ12 CPs (Fig. 7a). The whole printed microactuator can be carefully detached from the glass substrate by a micromanipulation setup. It is clear to observe that the microactuator contract along the alignment direction under the irradiation with the NIR laser (Fig. 7b, Video S1). To systematically characterize the response performance of the printed LCEs microstructures, maximum actuation strains of the microactuator on the glass substrate along $l_{\parallel}$ as the function of NIR laser power intensity are shown in Fig. 7c. The actuation strain (ε) is defined as

$$\varepsilon = \frac{L - l}{L} \tag{5}$$

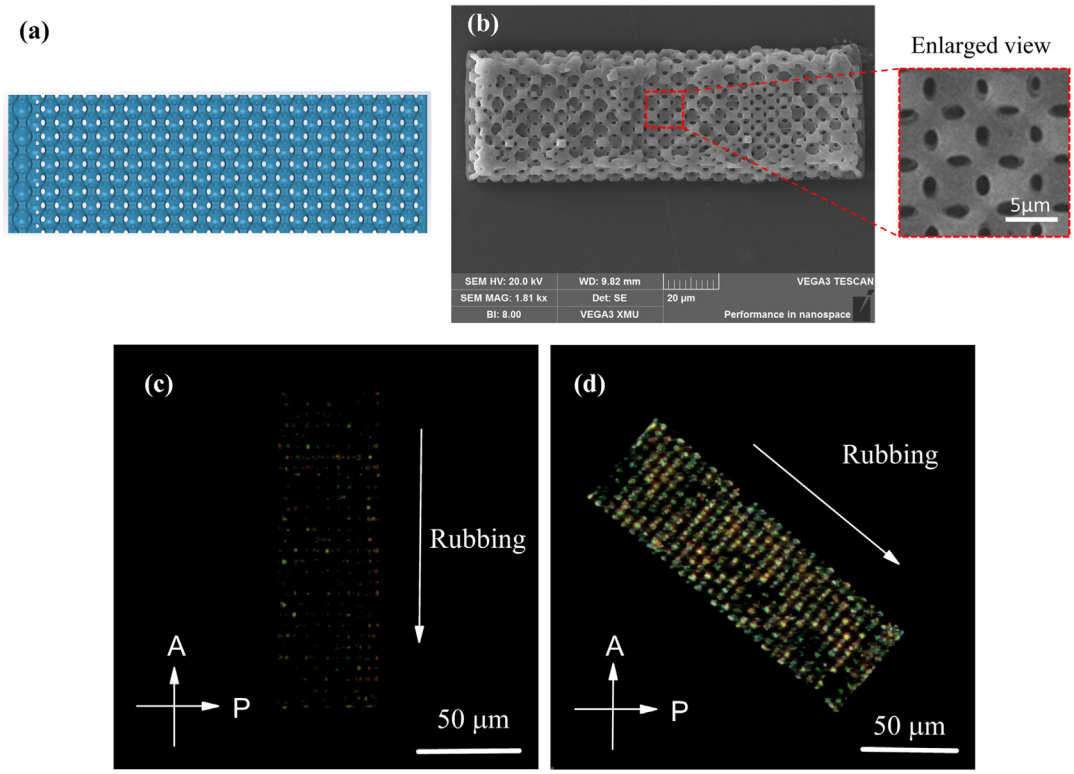

Fig. 6. (a) Top view of the designed microactuator composed of two layers of 3D inverse opal structure with 3.7 μm radius. (b) SEM image of porous 0.3 wt% CPs/LCEs microstructure. The inset is the enlarged view of the structures. (c-d) Polarized optical microscope pictures of the printed CPs/LCEs microstructures with the rubbing direction along the analyzer "A" and rotated by 45° with respect to the polarizer "P". The white arrows show the rubbing direction in the PI-coated glass. Scale bar: 50 μm.

where L is the length of the microactuator in the original state, whereas l is the length of the deformed microactuator in the actuated state. As shown in Fig. 7d, pristine LCEs microactuator without CPs showed neglectable actuation strains under different laser power intensities when the NIR laser power intensity rose from 47 to 173 mW/mm^2 at an interval of about 16 mW/mm^2. In contrast, the CPs/LCEs microactuator exhibited remarkable contraction strain values. Small actuation strain increases were observed as the NIR laser power intensity increased from 142 to 173 mW/mm^2. When the NIR laser power intensity was 173 mW/mm^2, the actuation strains of the CPs/LCEs microactuator reached the maximum values, 25.0% for the $l_{\parallel}$ direction and 13.6% for the $l_{\perp}$ direction (Fig. 7d, Video S2). A laser power intensity of 173 mW/mm^2 is advised as a suitable external stimulation value to assess the NIR photothermal actuation performance.

For the study on the effect of NIR laser power intensity on the response sensitivity of the soft microactuator, Fig. 7e shows the deformation and recovery time of the CPs/LCEs microactuator under NIR laser intensity of 94, 126, and 173 mW/mm^2. The microactuator displayed significantly different actuation performances at different laser power intensities. The contraction strains were 11, 20, and 25% when the power intensities were 94, 126, and 173 mW/mm^2, respectively. The microactuator could respond to the NIR laser quickly within 1 s. The microactuator could reach the maximum photo-induced actuation strain in 5 s under the NIR laser intensity of 173 mW/mm^2. Larger laser power intensity could trigger a shorter response time of the CPs/LCEs microactuator, which might be attributed to a higher local heating speed.

The photothermal actuation response of the porous CPs/LCEs microstructures to NIR light is fully reversible and reproducible for many actuation cycles. Periodic continuous NIR light on (5 s)/off (5 s) cycles was carried out to investigate the durability of the CPs/LCEs microactuator, and the results are shown in Fig. 7f. The actuator maintained the original uniaxial actuation strain ($\varepsilon \approx$ 25.0%) without obvious distortion after 100 cycles, indicating excellent anti-fatigue properties of the CPs/LCEs microstructure sample. The ability of microactuators to undergo significant reversible contraction strain is crucial in various functional devices and soft robotics applications. A larger contraction strain indicates the broader working range of the CPs/LCEs microactuators by controlling the external stimuli.

It is worth mentioning that the maximum contractile strain (25.0%) of the CPs/LCEs microactuator is higher than that of the previously reported DLW-TPP-printed light-responsive LCEs microactuators (20% for gold nanoparticles-incorporated LCEs woodpile microstructure under NIR laser [25], 20% for azobenzene-doped LCEs microstructure under 532 nm laser excitation [5], and 19% for azobenzene-filled LCEs micro-block under a green laser light [13]). With TPP-compatible CPs/LC photoresists, the fabrication of the light-responsive microactuators via DLW-TPP has been realized, and their excellent actuation performance under NIR light irradiation has also been demonstrated.

4. Conclusion

In summary, we have developed a new light-responsive LC photoresist that can be used in the precise construction of 3D micrometer-sized actuators via DLW-TPP technology. Different component ratios are carefully designed and tuned for room-temperature DLW-TPP. Conjugated polymers DPP58-TBZ12 with NIR absorption, high photothermal conversion efficiency (52.7%), and photostability were successfully synthesized via Stille cross-coupling polymerization to serve as the photothermal dopants. The CPs with D-A alternating backbone structures could be uniformly incorporated into LC photoresists to achieve the light response of the LC photoresists. And the CPs/LC photoresists could

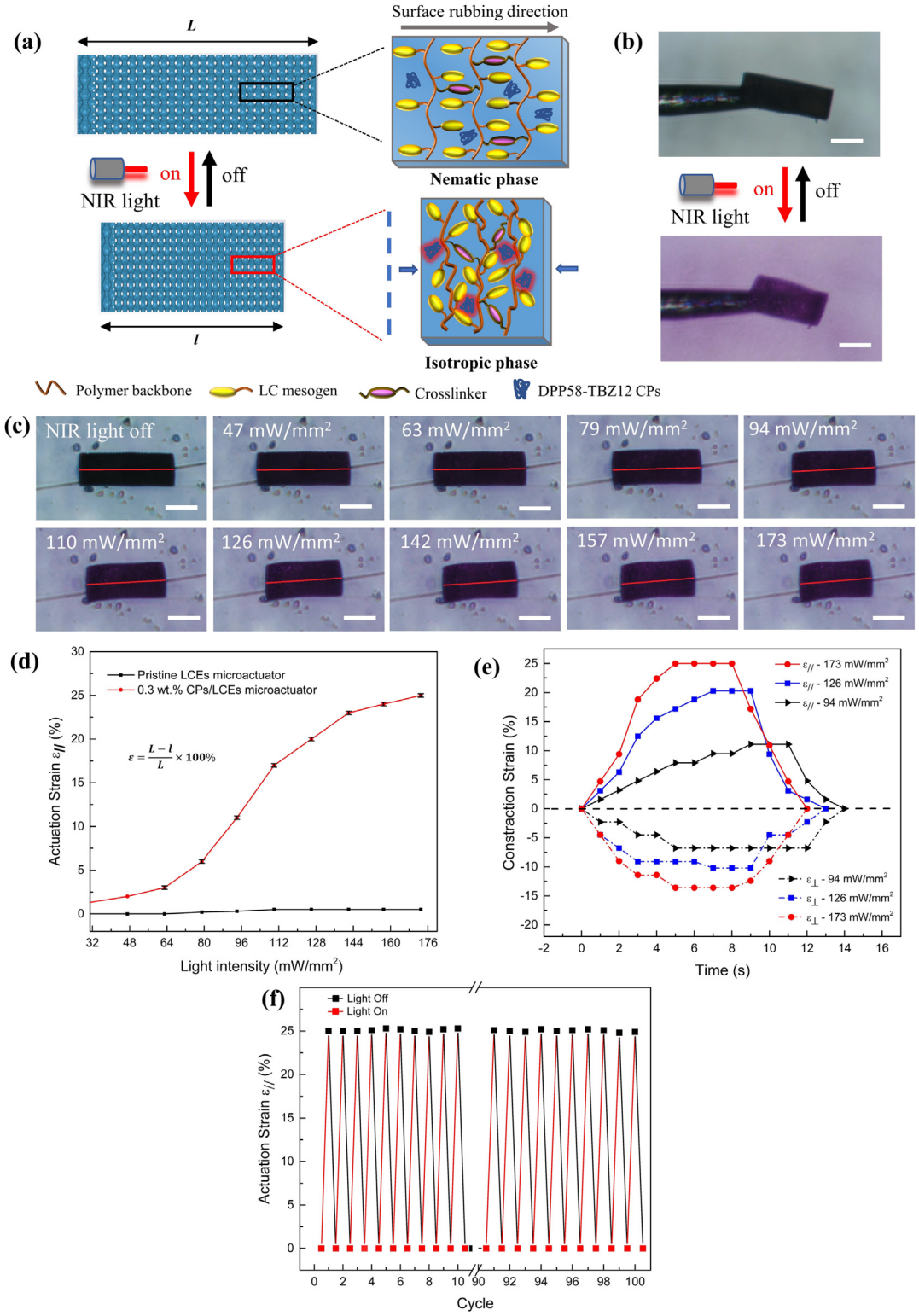

Fig. 7. (a) Schematic illustration shows reversible photothermal actuation styles of CPs/LCEs microactuators under an on–off switching of NIR light and corresponding reversible rearrangement mechanism of mesogens in LCEs polymeric network. (b) A microactuator is held on a steel tip in the air and illuminated by a NIR laser. Scale bar: 50 μm. (c) Photographs of microactuators in the equilibrium state under different NIR laser power intensities. Scale bar: 50 μm. (d) Maximum Actuation strain of the CPs/LCEs microactuator exposed to different laser power intensities. Error bars mean standard deviations for N = 3 measurements. (e) Actuation strain in the parallel and perpendicular directions as the function of time for the CPs/LCEs microactuator under different laser power intensities. (f) Reversible contraction strain of the microactuator triggered by the NIR light (808 nm, 173 mW/mm^2) on/off (ON: 5 s; OFF: 4 s).

maintain the room temperature liquid crystal phase stable for at least 7 days. The incorporation of CPs also lowered the T_{NI} value of the LC photoresists largely to alleviate some degrees of crystallization at room temperature, making them compatible with the commercial DLW-TPP without the need for a heating stage. By carefully tuning the photoresist formulation and printing parame-

ters (laser power and scanning speed), we demonstrate that the 4D microprinted porous CPs/LCEs microactuator with as low as 0.3 wt % CPs can achieve 25.0% actuation strain upon stimulation to NIR light (808 nm) of 173 mW/mm^2. The results demonstrate that the developed CPs/LC photoresists are promising materials for TPP-printable actuating micro-objects. This work enriches the choice library of DLW-TPP-compatible LC photoresists for fabricating responsive microactuators at room temperature. It is worth mentioning that the CPs/LC photoresists can also be applied to other 4D printing techniques like UV-assisted direct-ink-writing to manufacture macroscale structures, which paves the way toward the multi-scale 3D actuators with promising potential in the fields of functional separation membranes, and soft robotic systems and beyond.

Data availability

Data will be made available on request.

Declaration of Competing Interest

The authors declare that they have no known competing financial interests or personal relationships that could have appeared to influence the work reported in this paper.

Acknowledgments

The authors would like to thank the financial support from the Research Committee of The Hong Kong Polytechnic University (Project code: RK28). The work described in this paper was partially supported by a grant from the General Research Fund from the Research Grants Council of the Hong Kong Special Administrative Region, China (Project No. PolyU15211221).

Appendix A. Supplementary data

Supplementary data to this article can be found online at https://doi.org/10.1016/j.matdes.2023.112101.

References

[1] X. Bi, R. Huang, 3D printing of natural fiber and composites: A state-of-the-art review, Mater. Des. 222 (2022) 111065.
[2] F. Demoly, M.L. Dunn, K.L. Wood, H.J. Qi, J.-C. André, The status, barriers, challenges, and future in design for 4D printing, Mater. Des. 212 (2021) 110193.
[3] C. Liao, A. Wuethrich, M. Trau, A material odyssey for 3D nano/microstructures: two photon polymerization based nanolithography in bioapplications, Appl. Mater. Today 19 (2020) 100635.
[4] Z. Huang, G. Chi-Pong Tsui, Y. Deng, C.-Y. Tang, Two-photon polymerization nanolithography technology for fabrication of stimulus-responsive micro/nano-structures for biomedical applications, Nanotechnol. Rev. 9 (1) (2020) 1118–1136.
[5] H. Zeng, P. Wasylczyk, C. Parmeggiani, D. Martella, M. Burresi, D.S. Wiersma, Light-fueled microscopic walkers, Adv. Mater. 27 (26) (2015) 3883–3887.
[6] D. Martella, S. Nocentini, D. Nuzhdin, C. Parmeggiani, D.S. Wiersma, Photonic microhand with autonomous action, Adv. Mater. 29 (42) (2017) 1704047.
[7] Z. Xiong, C. Zheng, F. Jin, R. Wei, Y. Zhao, X. Gao, Y. Xia, X. Dong, M. Zheng, X. Duan, Magnetic-field-driven ultra-small 3D hydrogel microstructures: Preparation of gel photoresist and two-photon polymerization microfabrication, Sens. Actuators B 274 (2018) 541–550.
[8] T. Ritacco, D.M. Aceti, G. De Domenico, M. Giocondo, A. Mazzulla, G. Cipparrone, P. Pagliusi, Tuning cholesteric selective reflection in situ upon two-photon polymerization enables structural multicolor 4D microfabrication, Adv. Opt. Mater. 10 (2) (2022) 2101526.
[9] Y. Guo, H. Shahsavan, M. Sitti, Microscale polarization color pixels from liquid crystal elastomers, Adv. Opt. Mater. 8 (17) (2020) 1902098.
[10] A. Barbot, M. Power, F. Seichepine, G.-Z. Yang, Liquid seal for compact micropiston actuation at the capillary tip, Sci. Adv. 6 (22) (2020).
[11] Y.L. Zhang, Y. Tian, H. Wang, Z.C. Ma, D.D. Han, L.G. Niu, Q.D. Chen, H.B. Sun, Dual-3D femtosecond laser nanofabrication enables dynamic actuation, ACS Nano 13 (4) (2019) 4041–4048.
[12] J.-Y. Wang, F. Jin, X.-Z. Dong, J. Liu, M.-L. Zheng, Flytrap inspired pH-driven 3D Hydrogel actuator by femtosecond laser microfabrication, Adv. Mater. Technol. 7 (8) (2022) 2200276.
[13] D. Martella, D. Antonioli, S. Nocentini, D.S. Wiersma, G. Galli, M. Laus, C. Parmeggiani, Light activated non-reciprocal motion in liquid crystalline networks by designed microactuator architecture, RSC Adv. 7 (32) (2017) 19940–19947.
[14] M. del Pozo, C. Delaney, M. Pilz da Cunha, M.G. Debije, L. Florea, A.P.H.J. Schenning, Temperature-responsive 4D liquid crystal microactuators fabricated by direct laser writing by two-photon polymerization, Small Struct. 3 (2) (2022) 2100158.
[15] H. Yang, G. Ye, X. Wang, P. Keller, Micron-sized liquid crystalline elastomer actuators, Soft Matter 7 (3) (2011) 815–823.
[16] C. Zheng, F. Jin, Y. Zhao, M. Zheng, J. Liu, X. Dong, Z. Xiong, Y. Xia, X. Duan, Light-driven micron-scale 3D hydrogel actuator produced by two-photon polymerization microfabrication, Sens. Actuators B 304 (2020) 127345.
[17] X. Wang, X.-H. Qin, C. Hu, A. Terzopoulou, X.-Z. Chen, T.-Y. Huang, K. Maniura-Weber, S. Pané, B.J. Nelson, 3D printed enzymatically biodegradable soft helical microswimmers, Adv. Funct. Mater. 28 (45) (2018) 1804107.
[18] C.P. Ambulo, J.J. Burroughs, J.M. Boothby, H. Kim, M.R. Shankar, T.H. Ware, Four-dimensional printing of liquid crystal elastomers, ACS Appl. Mater. Interfaces 9 (42) (2017) 37332–37339.
[19] Y. Cheng, K. Ren, D. Yang, J. Wei, Bilayer-type fluorescence hydrogels with intelligent response serve as temperature/pH driven soft actuators, Sens. Actuators B 255 (2018) 3117–3126.
[20] M. Ilami, H. Bagheri, R. Ahmed, E.O. Skowronek, H. Marvi, Materials, actuators, and sensors for soft bioinspired robots, Adv. Mater. 33(19) (2021) e2003139.
[21] H. Yang, A. Buguin, J.-M. Taulemesse, K. Kaneko, S. Méry, A. Bergeret, P. Keller, Micron-sized main-chain liquid crystalline elastomer actuators with ultralarge amplitude contractions, J. Am. Chem. Soc. 131 (41) (2009) 15000–15004.
[22] A. Buguin, M.-H. Li, P. Silberzan, B. Ladoux, P. Keller, Micro-actuators: when artificial muscles made of nematic liquid crystal elastomers meet soft lithography, J. Am. Chem. Soc. 128 (4) (2006) 1088–1089.
[23] Y. Wang, R. Yin, L. Jin, M. Liu, Y. Gao, J. Raney, S. Yang, 3D-printed photoresponsive liquid crystal elastomer composites for free-form actuation, Adv. Funct. Mater. 33 (4) (2023) 2210614.
[24] L.-Y. Hsu, P. Mainik, A. Münchinger, S. Lindenthal, T. Spratte, A. Welle, J. Zaumseil, C. Selhuber-Unkel, M. Wegener, E. Blasco, A facile approach for 4D microprinting of multi-photoresponsive actuators, Adv. Mater. Technol. 8 (1) (2023) 2200801.
[25] L. Chen, Y. Dong, C.Y. Tang, L. Zhong, W.C. Law, G.C.P. Tsui, Y. Yang, X. Xie, Development of direct-laser-printable light-powered nanocomposites, ACS Appl. Mater. Interfaces 11 (21) (2019) 19541–19553.
[26] X. Lu, S. Guo, X. Tong, H. Xia, Y. Zhao, Tunable photocontrolled motions using stored strain energy in malleable azobenzene liquid crystalline polymer actuators, Adv. Mater. 29 (28) (2017) 1606467.
[27] T. Ikeda, J. Mamiya, Y. Yu, Photomechanics of liquid-crystalline elastomers and other polymers, Angew. Chem. Int. Ed. Engl. 46 (4) (2007) 506–528.
[28] Y. Wang, A. Dang, Z. Zhang, R. Yin, Y. Gao, L. Feng, S. Yang, Repeatable and reprogrammable shape morphing from photoresponsive gold nanorod/liquid crystal elastomers, Adv Mater 32(46) (2020) e2004270.
[29] W. Wang, X. Sun, W. Wu, H. Peng, Y. Yu, Photoinduced deformation of crosslinked liquid-crystalline polymer film oriented by a highly aligned carbon nanotube sheet, Angew. Chem. Int. Ed. Engl. 51 (19) (2012) 4644–4647.
[30] W. Xiong, Y. Liu, L.J. Jiang, Y.S. Zhou, D.W. Li, L. Jiang, J.F. Silvain, Y.F. Lu, Laser-directed assembly of aligned carbon nanotubes in three dimensions for multifunctional device fabrication, Adv. Mater. 28 (10) (2016) 2002–2009.
[31] M. Del Pozo, J. Sol, A. Schenning, M.G. Debije, 4D printing of liquid crystals: what's right for me?, Adv. Mater. 34(3) (2022) e2104390.
[32] X. Men, H. Chen, C. Sun, Y. Liu, R. Wang, X. Zhang, C. Wu, Z. Yuan, Thermosensitive polymer dot nanocomposites for trimodal computed tomography/photoacoustic/fluorescence imaging-guided synergistic chemo-photothermal therapy, ACS Appl. Mater. Interfaces 12 (46) (2020) 51174–51184.
[33] H.J. Kim, B. Kim, Y. Auh, E. Kim, Conjugated organic photothermal films for spatiotemporal thermal engineering, Adv. Mater. (2021) e2005940.
[34] W. Liu, L.-X. Guo, B.-P. Lin, X.-Q. Zhang, Y. Sun, H. Yang, Near-infrared responsive liquid crystalline elastomers containing photothermal conjugated polymers, Macromolecules 49 (11) (2016) 4023–4030.
[35] Z. Huang, G.-C.-P. Tsui, Y. Deng, C.-Y. Tang, M. Yang, M. Zhang, W.-Y. Wong, Bioinspired near-infrared light-induced ultrafast soft actuators with tunable deformation and motion based on conjugated polymers/liquid crystal elastomers, J. Mater. Chem. C 10 (35) (2022) 12731–12740.
[36] K.-W. Yeung, Y. Dong, L. Chen, C.-Y. Tang, W.-C. Law, G.C.-P. Tsui, D.S. Engstrøm, Printability of photo-sensitive nanocomposites using two-photon polymerization, 9(1) (2020) 418-426.
[37] Y. Guo, H. Shahsavan, M. Sitti, 3D Microstructures of Liquid Crystal Networks with Programmed Voxelated Director Fields, Adv Mater 32(38) (2020) e2002753.
[38] D. Liu, D.J. Broer, Liquid crystal polymer networks: preparation, properties, and applications of films with patterned molecular alignment, Langmuir 30 (45) (2014) 13499–13509.
[39] D.L. Meyer, N. Schmidt-Meinzer, C. Matt, S. Rein, F. Lombeck, M. Sommer, T. Biskup, Side-chain engineering of conjugated polymers: distinguishing its impact on film morphology and electronic structure, J. Phys. Chem. C 123 (33) (2019) 20071–20083.

[40] D.K. Roper, W. Ahn, M. Hoepfner, Microscale heat transfer transduced by surface plasmon resonant gold nanoparticles, J. Phys. Chem. C 111 (9) (2007) 3636–3641.
[41] X. Liu, L. Kong, H. Du, Y. Zhang, J. Zhao, Y. Xie, Synthesis and electrochromic properties of electrochromic polymers based on propylenedioxythiophene, diketopyrrolopyrrole and benzodithiophene units, Org. Electron. 64 (2019) 223–235.
[42] P. Chen, Y. Ma, Z. Zheng, C. Wu, Y. Wang, G. Liang, Facile syntheses of conjugated polymers for photothermal tumour therapy, Nat. Commun. 10 (1) (2019) 1192.
[43] T. Sun, J.H. Dou, S. Liu, X. Wang, X. Zheng, Y. Wang, J. Pei, Z. Xie, Second near-infrared conjugated polymer nanoparticles for photoacoustic imaging and photothermal therapy, ACS Appl. Mater. Interfaces 10 (9) (2018) 7919–7926.
[44] Y. Du, Y. Ding, F. Ge, X. Wang, S. Ma, H. Lu, G. Zhang, L. Qiu, A regular ternary conjugated polymer bearing π-extended diketopyrrole and isoindigo acceptor units for field-effect transistors and photothermal conversion, Dyes Pigm. 164 (2019) 27–34.
[45] F. Sugiyama, A.T. Kleinschmidt, L.V. Kayser, D. Rodriquez, M. Finn 3rd, M.A. Alkhadra, J.M. Wan, J. Ramirez, A.S. Chiang, S.E. Root, S. Savagatrup, D.J. Lipomi, Effects of flexibility and branching of side chains on the mechanical properties of low-bandgap conjugated polymers, Polym. Chem. 9 (33) (2018) 4354–4363.
[46] J.M. McCracken, B.R. Donovan, K.M. Lynch, T.J. White, Molecular engineering of mesogenic constituents within liquid crystalline elastomers to sharpen thermotropic actuation, Adv. Funct. Mater. 31 (16) (2021) 2100564.
[47] T.S. Hebner, C.N. Bowman, T.J. White, The contribution of intermolecular forces to phototropic actuation of liquid crystalline elastomers, Polym. Chem. 12 (10) (2021) 1581–1587.